MagnetoSuture: Tetherless Manipulation of Suture Needles

Lamar O. Mair, *Member, IEEE*, Xiaolong Liu, *Member, IEEE*, Bhargav Dandamudi, *Member, IEEE*, Kamakshi Jain, Sagar Chowdhury, *Member, IEEE*, Jeremy Weed, Yancy Diaz-Mercado, *Member, IEEE*, Irving N. Weinberg, *Member, IEEE*, and Axel Krieger, *Member, IEEE*

***Abstract*—This paper demonstrates the feasibility of ligation and tissue penetration for surgical suturing tasks using magnetically actuated suture needles. Manipulation of suture needles in minimally invasive surgery involves using articulated manual/robotic tools for needle steering and controlling needle-tissue or thread-tissue interactions. The large footprints of conventional articulated surgical tools significantly increase surgical invasiveness, potentially leading to longer recovery times, tissue damage, scarring, or associated infections. Aiming to address these issues, we investigate the feasibility of using magnetic fields to tetherlessly steer suture needles. The primary challenge of such a concept is to provide sufficient force for tissue penetration and ligation. In this work, we demonstrate proof-of-concept capabilities using the MagnetoSuture system, performing tissue penetration and ligation tasks using *ex vivo* tissues, customized NdFeB suture needles with attached threads, and remote-controlled magnetic fields. To evaluate the system performance, we conducted experiments demonstrating tetherless recreation of a purse string suture pattern, ligation of an excised segment of a rat intestine, and penetration of rat intestines.**

***Index Terms*—Electromagnetic system, magnetic control, magnetic needle steering, suture, tissue penetration, tissue ligation.**

I. Introduction

SUTURING and ligation are critical and technically challenging aspects of most surgeries from cardiovascular to gastrointestinal surgery. Well over a million anastomoses using suturing are performed in the USA each year for visceral indications alone (gastrointestinal, urologic and gynecologic surgery) [1], [2]. Suturing and ligation have historically relied on articulated, physical manipulation of the suture device or suture needle [3]. Minimally invasive surgical procedures have involved inserting miniature manipulators into the patient's body via a single incision [4] or natural orifices [5]. For some procedures, surgeons can teleoperate the miniature manipulators with dexterous robotic tools as the end-effectors to carry out complex suturing tasks, which results in shorter hospital stays and faster recoveries [6]. Advances in computer vision, path planning, and mechanical force feedback sensing are enabling robotic tools capable of suturing and ligating with improved precision and decreasing involvement from human surgeons [7].

For surgeries requiring suturing or ligation, the procedure makes use of a suture needle, suture thread, and surgical manipulator (e.g., manual or robotic laparoscopic needle driver) for guiding the needle. Of these objects, the surgical manipulators have the largest mechanical footprint in the patient, making the manipulators the most invasive components used in the procedure. Minimizing the invasiveness of surgery is an important goal of surgical robotics. Manipulators used for guiding needles during surgery have the potential to 1) cause damage to tissues, 2) cause infections at surgical site, and 3) result in large scars [8]. As such, removing manipulators alleviates these potential sources of complications.

Instead of tactile manipulation of needles, access to the target tissue could be achieved by percutaneous insertion of the suture needle and subsequent magnetic manipulation to the target. The ability to suture and ligate in a non-contact manner would significantly decrease the invasiveness and associated trauma of a procedure. Given it can be performed with adequate fidelity and under sufficient motion control, a tetherless approach may decrease complications and reduce recovery time. Tetherless robotic tool manipulation in which torques and forces are provided by magnetic field offers a potential route to minimally invasive surgery. Procedures enabled by such a magnetic manipulation technique could include truly minimally invasive repairs of hernias, vaginal prolapse, or emergency procedures to stop a hemorrhage.

The field of magnetically manipulated microscale rods [9], [10], helices [11]–[13], and surface walkers [14]–[17] has produced elaborate work focused on medical applications inside the body and on tissues [18]–[20]. Recent research has aimed at steering millimeter-scale tools on the eye for diagnosis, including application of magnetic force for assessing vitreous pressure [21], [22]. The field of magnetic catheter guidance has advanced to clinical use, with several companies having magnetic catheter guidance systems installed

Manuscript received January 13, 2020; revised February 26, 2020 and March 27, 2020; accepted April 6, 2020. Date of publication April 17, 2020; date of current version May 20, 2020. This article was recommended for publication by Associate Editor T. Haidegger and Editor P. Dario upon evaluation of the reviewers' comments. This work was supported in part by the Fischell Institute for Medical Devices and the University of Maryland Medical Device Development Fund, and in part by the National Institute of Biomedical Imaging and Bioengineering of the National Institutes of Health under Award R01EB020610. *(Corresponding author: Axel Krieger.)*

Lamar O. Mair, Sagar Chowdhury, and Irving N. Weinberg are with the Division of Magnetic Manipulation and Particle Research, Weinberg Medical Physics, Inc., North Bethesda, MD 20852 USA (e-mail: lamar.mair@gmail.com).

Xiaolong Liu, Bhargav Dandamudi, Kamakshi Jain, Jeremy Weed, Yancy Diaz-Mercado, and Axel Krieger are with the Department of Mechanical Engineering, University of Maryland, College Park, MD 20742 USA, and also with the Maryland Robotics Center, University of Maryland, College Park, MD 20742 USA (e-mail: axel@umd.edu).

This article has supplementary downloadable material at http://ieeexplore.ieee.org, provided by the authors.

Digital Object Identifier 10.1109/TMRB.2020.2988462

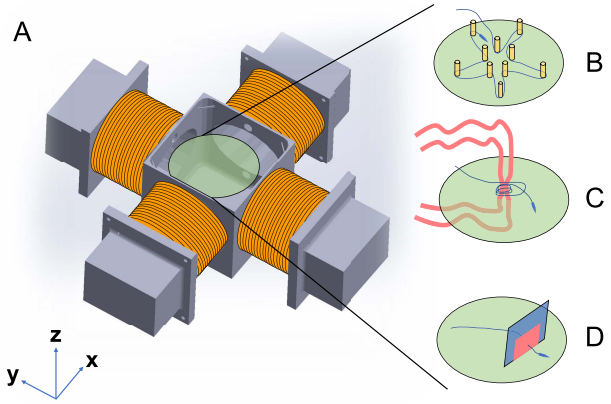

Fig. 1. (A) Schematic drawing showing manipulation coil array and highlighted manipulation area. (B) Schematic of purse string suture pattern. (C) Schematic drawing showing ligation of tubular intestine tissue. (D) Schematic drawing showing tissue penetration.

around the world [23], [24], and Chautems and Nelson demonstrated exquisite 5-degree of freedom control over a permanent magnet attached to a catheter tube by a highly flexible tether [25]. However, less work has been performed on magnetic manipulation of millimeter and centimeter scale tools with attached threads for suturing and ligation applications. Additionally, much of the work on magnetically guided millimeter/centimeter scale tools focuses on using rotating magnetic fields for manipulating helical or corkscrew-style devices [26]–[28], which drill through the tissue phantoms and excised tissues under an applied magnetic torque [27]–[32]. These rotating methods of manipulation are useful and enable effective control and tissue penetration. However, it is unclear whether or not using twisting motion to induce transport through tissues so as to penetrate the tissues will induce excessive tissue damage compared with pulling a magnetic suture needle through the tissue, an action which more naturally replicates current surgical practice. In addition, continuous rotation of a suture needle with attached thread can lead to undesirable thread knotting. One major barrier to implementation is achieving sufficient force for tissue penetration and ligation. Leclerc *et al.* achieved penetration through sheep brain by hammering a millibot into the soft brain tissue using an onboard spring and a magnetic ball placed inside a hollow cavity in the robot body [33]. However, the penetration of other types of tissues by magnetically actuated needles is still unsolved.

In this paper we demonstrate a system capable of performing the aforementioned tasks *in vitro* using *ex vivo* tissues and a sharpened NdFeB suture needle guided by magnetic fields, as conceptually illustrated in Fig. 1. In our MagnetoSuture system magnetic fields and gradients are supplied by an electromagnet array which is controlled using a hand-held remote controller. The contributions of this paper include demonstration of the ability to tetherlessly recreate a purse string suture pattern (Fig. 1B), ligation of an excised segment of rat intestine (Fig. 1C), and penetration of rat intestine via magnetic pulling only (Fig. 1D). To the best of our knowledge, this work presents the first demonstration of tissue penetration using a customized suture needle and thread guided using only magnetic gradient pulling. We also demonstrate the formation of a complex, medically relevant suture pattern performed tetherlessly using a suture needle with thread. Additional contributions include characterization of the force needed to penetrate rat intestine, pig intestine, and synthetic tissue using our custom magnetic needle and a comparison of our custom NdFeB needle with a clinical suture needle.

II. Methods

The design of the MagnetoSuture system was guided by the need to generate sufficient force on a needle to ligate and penetrate tissues via pulling a needle through the tissue. Of these two tasks, penetration requires significantly more force, and so preliminary measurements and calculations of the force required for penetration were performed to guide system design. Below, we describe our process for designing our NdFeB needle. Following, we describe tissue penetration force assessments performed using force sensors in which we compare the force required to penetrate various tissues using our NdFeB needle as compared with a commercially available suture needle (Ethicon ST-4). Ethicon ST-4 needles are 19.5 mm long and 0.6 mm in diameter. NdFeB needles are approximately 25.4 mm long and 1.6 mm in diameter. The force assessment results were used to guide the design of our electromagnet coil array. Finally, we describe the needle controller and associated hardware before describing experiments and presenting results.

A. NdFeB Needle Design

To a reasonable approximation, the magnetic force $\mathbf{F}_m$ on a uniformly magnetized object is described by the volume and magnetization of the object, and the gradient of external magnetic field applied

$$\mathbf{F}_m = \nu \nabla (\mathbf{M} \cdot \mathbf{B}) \tag{1}$$

where ν represents the volume of the magnetic object, ∇ is the gradient operator, $\mathbf{M}$ represents the remanent magnetization vector of the object, $\cdot$ is the dot product operator, and $\mathbf{B}$ is the magnetic field applied to the object [34].

Our ideal NdFeB needle would maintain a strong remanent magnetization, be uniformly magnetized, sharp, and have a well-attached suture needle thread. Commercial needles, e.g., the Ethicon ST-4 needle as illustrated on the left side of Fig. 2, are commonly made from medical grade austenitic SAE 316 stainless steel. This steel is magnetically soft and has a naturally low magnetic permeability and a low remanent magnetization. Consequently, large field gradients are necessary to achieve significant magnetic force.

Alternatively, for the purpose of magnetic manipulation, magnetically hard materials such as neodymium iron boron (NdFeB) have large, stable remanent magnetizations, possibly making them ideal for use as NdFeB suture needles guided by a MagnetoSuture system. To explore this possibility, we fashioned NdFeB needles from 1.6 mm diameter NdFeB cylinders, forming needles by sharpening the cylinder end using a high speed rotating tool and sand paper (400 and 2000 grit). Notable differences in needle sharpness can be seen in Fig. 2, which

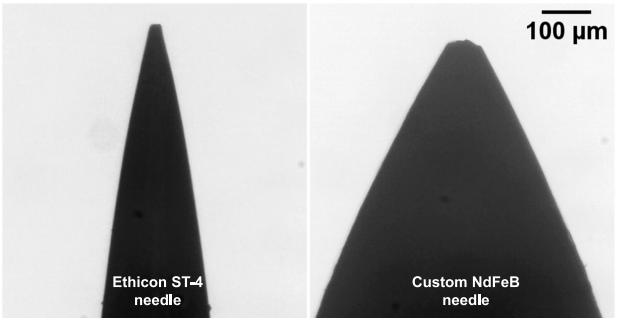

Fig. 2. Images of commercial Ethicon ST-4 needle (left) and custom NdFeB needle (right) tips. Images were collected using a 4x microscope objective under transmitted light microscopy conditions.

shows a commercial Ethicon ST-4 needle tip (left) beside our sharpened NdFeB MagneoSuture needle (right).

B. Tissue Penetration Force Assessment

In order to design a system capable of accomplishing tissue penetration via magnetic force pulling alone, we first obtained estimates of the force required to penetrate three model tissues: rat intestine, pig intestine, and synthetic saphenous vein (3-Dmed, Inc.; www.3-dmed.com). Typically, tissue penetration requires between 0.03 N to 1.95 N, depending on the tissue's mechanical properties and needle sharpness [35]. A major challenge for penetrating tissues using forces which replicate standard pushing/pulling suturing protocol is the application of sufficient force to penetrate tissues.

To measure the required force for penetration for two types of needles (Ethicon ST-4 needle and NdFeB needle, as illustrated in Fig. 2), we mounted the needles on a one degree of freedom (DOF) mechanical testing system, as illustated in Fig. 3A. A vertical actuator was equipped with a six DOF force/torque sensor (Nano17, ATI Industrial Automation; www.ati-ia.com) to measure the force acting on the needle while the needle was mounted on a chuck and pushed into a suspended tissue sample. The ATI Nano17 force/torque sensor has force sensing resolution of 3.125 mN. A motorized translation stage (PT1-Z8-25mm, Thorlabs; www.thorlabs.com) with a displacement resolution of 29 nm was used to maintain a constant velocity during penetration experiments. Using the system to measure forces at 10 Hz, we inserted needles into tissue samples until tissue penetration was accomplished.

Fig. 3B shows the force on a needle as a function of time, with the force growing as the needle contacts the tissue surface and pushes into the tissue, increasing further until the tissue is punctured (Fig. 3B: P1, P2, and P3). For rat intestine penetration force tests, the intestine was mounted in its tubular form and the needle was pushed through both layers of the intestine wall. Importantly, here we see a significant difference in tissue penetration behavior based on the sharpness and diameter of the respective needles. The Ethicon ST-4 needle penetrates both layers of the intestine with ease (approximately 0.15 N) and little to no discrepancy is observed for the penetration force required to push the needle through the second layer, as compared to the force required for penetrating the first layer. The NdFeB needle, on the other hand, being significantly

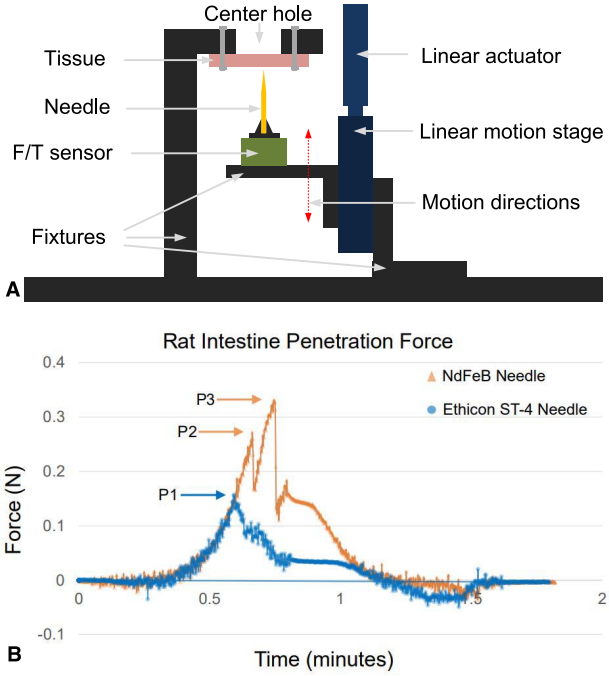

Fig. 3. Penetration force measurements for Ethicon ST-4 and NdFeB needles to penetrate through rat intestine tissue. (A) The experimental platform setup for measuring needle penetration forces. (B) Representative penetration force measurement data. There are three points of interest, indicated by labeled arrows P1, P2, and P3. P1 indicates penetration point for the Ethicon ST-4 suture needle. The sharpness of the Ethicon needle is such that both layers of the intestine are penetrated immediately, at the same force. P2 indicates the force at which the first layer of intestine is penetrated by the NdFeB needle, and P3 indicates the force at which the second layer of intestine is penetrated by the NdFeB needle.

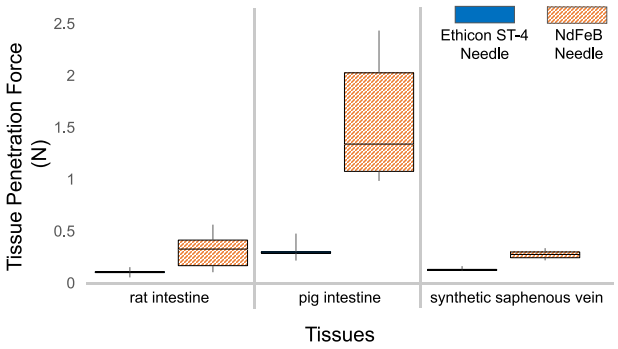

Fig. 4. Comparison of required tissue penetration forces between Ethicon ST-4 and NdFeB needles by testing on different tissue samples (left to right): rat intestine, pig intestine, and synthetic saphenous vein.

less sharp and wider in diameter, requires significantly greater force to penetrate the first layer of the intestine (approximately 0.28 N), and requires further force (approximately 0.32 N) to penetrate the second layer of the intestine.

Fig. 4 statistically compares the penetration forces between the two needles for penetrating three different types of sample tissues: rat intestine, pig intestine, and synthetic saphenous vein. To investigate if significant differences exist between the Ethicon ST-4 needle and the NdFeB needle for tissue penetration, we conducted two-sample t-tests by giving the null hypothesis as $\mu_s = \mu_m$, where μ_s and μ_m represent the mean values of penetration forces by the Ethicon ST-4 needle and the NdFeB needle in each sample test.

According to the data shown in Fig. 4 and the two-sample t-test results, the median penetration forces required by the Ethicon ST-4 needle and the NdFeB needle are 0.11 N and 0.33 N respectively with p-value computed as 0.01 from the two-sample t-test for the case of rat intestine, 0.29 N and 1.34 N respectively with p-value as 6.94×10^{-4} for the case of pig intestine, and 0.13 N and 0.28 N respectively with p-value as 1.41×10^{-7} for the case of synthetic saphenous vein. The tissue type and associated mechanical properties affect the required penetration force, with pig intestine requiring significantly more penetration force compared to rat intestine and synthetic veins. It is also worth noting that porcine intestine is significantly more variable in its required penetration force, possibly due to significant variability at the millimeter and centimeter scale in the organization, density, and thickness of the tissue. Thus, we anticipate various segments of the pig intestine embody highly variable mechanical properties, inducing considerable variability in required penetration force. Such variability is significantly less apparent for the rat intestine.

The experiments consistently indicate that for the same tissue more force is required to achieve tissue penetration using our custom NdFeB needle than is required for penetration by the Ethicon ST-4 needle. This significant peak force difference is caused by the differences in sharpness and needle diameter, illustrated in Fig. 2. Future studies would benefit from a sharper NdFeB needle. In this work, the measured penetration forces from the NdFeB needle were used to design the electromagnetic array in order to generate sufficient magnetic force for rat intestine tissue penetration according to Equation (1).

C. Electromagnetic Array Design

We propose a cube-shaped magnetic work space greater than 90 mm × 90 mm with the ability to generate sufficient force on a NdFeB needle to demonstrate tissue penetration. In particular, we created an electromagnetic coil array containing four coils, each coil having an outer diameter of 98 mm. The coils are orthogonally arranged along the X and Y axes with an optional insertable soft iron core to enhance the magnetic field. A picture of the coil array is shown in Fig. 5. Coils were wound on a 3D printed ULTEM 1010 frame (Stratasys Direct; www.stratasysdirect.com), ULTEM 1010 being chosen for its comparatively high heat deflection temperature (217 °C). Coils were wound using AWG 16 polyimide-coated copper wire (MWS Wire Industries, Inc.; www.mwswire.com) and had lengths of 60 mm, inner diameters of 85 mm, and outer diameters of 98 mm, as shown in Fig. 6. Each coil had 54 turns per layer, 12 layers, and a total resistance ≈2.7 Ω. The iron cores for each coil, when used, were identical as well, having diameters of 50.8 mm, lengths of 66 mm, and relative permeability of approximately 3000. We have confined these initial experiments to two-dimensional manipulations of our NdFeB needle, all manipulations taking place in a circular Petri dish. To cool coils during operation, the system was placed in a circulating chilled water bath, which submerged approximately half of each coil in flowing water <5 °C. The chilled water bath was created by flowing water into and out of a shallow polyethylene pan with faucet (McMaster Carr, 3744K12).

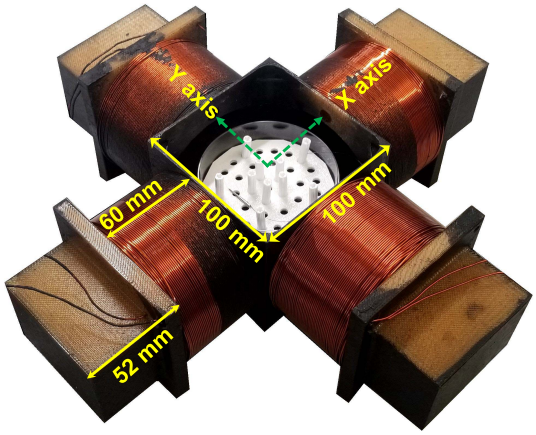

Fig. 5. A four coil array was printed from ULTEM 1010 (Stratasys Direct) and coils were directly wound onto the printed form. The interior surface of the printed form was coated with a waterproof resin sealant to prevent water leaking into the sample region of interest. Here, an inserted sample dish and pegs for purse string suture pattern are shown.

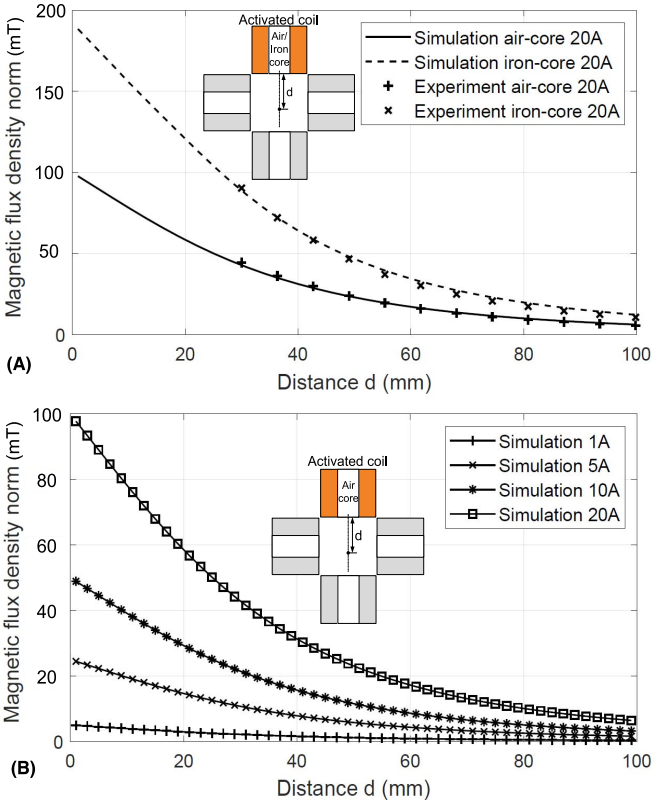

Fig. 6. Electromagnetic array magnetic field modeling and validation. (A) Comparison of experimental measurements and simulation results. (B) Simulations of the magnetic field along the central axis of a single air core coil.

The pan had interior dimensions of 49.4 cm × 39.1 cm × 7.1 cm. Water was chilled by extracting water from a 38 liter reservoir filled with ice and water. No closed loop control of temperature was used.

According to the NdFeB needle in Section II-A and the tissue penetration forces measured in Section II-B, we designed the electromagnetic coils using finite element method (FEM) simulation (COMSOL4.3) to satisfy the design requirements.

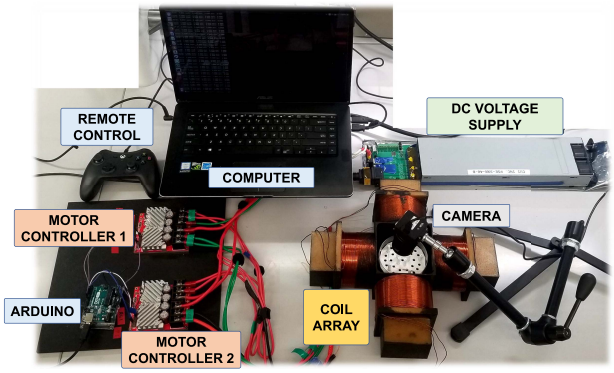

Fig. 7. System overview showing power, control, steering, manipulation, and video acquisition components.

Guided by the mechanically measured penetration force data, magnetic properties of NdFeB magnets, and reasonable dimensions for a NdFeB needle with lengths similar to common suture needles, we predicted the required fields and gradients created by our MagnetoSuture system for accomplishing tissue penetration. For needle diameters of 1.6 mm, a needle 20 mm to 30 mm in length would experience sufficient force to penetrate rat intestine in a system capable of generating about 50 mT at the center of the cubic volume. Our system becomes sufficiently strong to accomplish intestine penetration using a single coil supplied with 20 A and an iron core.

Fig. 6 demonstrates the analysis of the generated magnetic field from the proposed electromagnetic array by using both FEM and experiment measurements. The magnetic flux density norm $|\mathbf{B}|$ along one activated coil a centerline distance d from the coil was first simulated by using a 20 A current input with both air core and iron core configurations in the coil. Under the same configurations, we then experimentally measured $|\mathbf{B}|$ along the coil's center line using a Gauss meter (GM3, AlphaLab Inc.; www.alphalabinc.com). Fig. 6A shows the comparison of the simulated and measured magnetic field flux norms with respect to d, which indicate accurate prediction of the magnetic field by using FEM. In addition, we can observe that by inserting an iron core inside the coil and supplying 20 A current, the value of $|\mathbf{B}|$ is 46.7 mT at $d = 50$ mm. Although $|\mathbf{B}(d = 50\,\text{mm})|$ is slightly smaller than 50 mT by activating one coil, the maximum value of $|\mathbf{B}(d = 50\,\text{mm})|$ is doubled as 93.4 mT by activating the opposite two coils simultaneously. In Fig. 6B, we demonstrate the simulated magnetic flux density norm for a single air core coil by varying input currents of 1 A, 5 A, 10 A, and 20 A. Within the nearest 20 mm to the coil, our system generates an average gradient of $\approx$ 2,778 mT/m when operated at 20 A with an iron core.

D. NdFeB Needle Controller

Fig. 7 shows the configuration of the control system for the eletromagnetic array. The input currents into the four coils were controlled using two dual-channel motor controllers (RoboClaw, Basic Micro; www.basicmicro.com) with pulse width modulation. The motor drivers were powered by an AC-DC converter capable of supplying 54 V and 55 A (MeanWell USA PSE-3000-54-F; www.meanwellusa.com). Each coil was enabled for bipolar operation, and each coil was controlled independently by two pairs of two-axis joysticks (AmazonBasics Xbox One Wired Controller; www.amazon.com), which communicated with the motor controllers via microcontroller (UNO R3, Arduino; www.arduino.cc). Each axis on a single joystick enabled bipolar control over a single coil. For all experiments, samples were placed in 85 mm diameter Petri dishes. Imaging feedback was performed by a camera (Chameleon CMLN-13S2C, FLIR systems, Inc.; www.flir.com), positioned above the Petri dish, imaging at 15 frames per second.

All experiments were conducted using custom NdFeB needles (1.6 mm wide) made from cylindrical N42 grade NdFeB magnets magnetized along the long axis (K&J Magnetics; www.kjmagnetics.com), as discussed in Section II-A. Various NdFeB needles with different lengths were used for the various experiments, as some experiments required maximum needle force while other experiments required maximum needle manueverability. For example, longer NdFeB needles were used for ligation and tissue penetration experiments so as to maximize the force on the needles, while shorter NdFeB needles were used for navigation in crowded spaces, such as the purse string suture pattern formation. Suture thread was attached to the NdFeB needle using a general adhesive.

To demonstrate how the electromagnetic array is controlled for actuating the NdFeB needle, magnetic field maps in the Petri dish area are simulated and illustrated in Fig. 8 by activating different coils. To simplify control, we activate the coils to control the needle along the four cardinal directions and the four diagonal directions in between (total of eight directions). By activating one single coil (or two opposing coils), the NdFeB needle will align with the magnetic field directions (white arrows), and move in those directions, as shown in Fig. 8A-D. For actuating the needle to move in diagonal directions, two adjacent coils are activated with equal input currents, as shown in Fig. 8E-H. The top and bottom left figures in Fig. 8 illustrate the magnetic flux density norm distributions of the cases shown in Fig. 8A and Fig. 8E, respectively.

Having generated NdFeB needles, compared their required tissue penetration forces with commercial suture needles, modeled the required magnetic fields and gradients needed for penetrating rat intestine, and described our magnetic manipulation system and hardware, we next present experiments and results performed using the NdFeB needles and manipulation system.

III. Experiments and Results

A. NdFeB Needle Steering Experiments

1) Purse String Suture Pattern: The purse string suture [36] is a special type of suture pattern for closing organs and wounds with broad application in surgical [37], gynecological [38], urological [39], and dermatological [40] procedures. In this experiment, we recreate a purse string suture pattern in 2D, demonstrating the ability to overcome the friction generated by suture thread being pulled over ten friction-inducing points of contact using the MagnetoSuture system. In this experiment (Fig. 9), we demonstrate the ability to overcome the friction generated by suture thread being

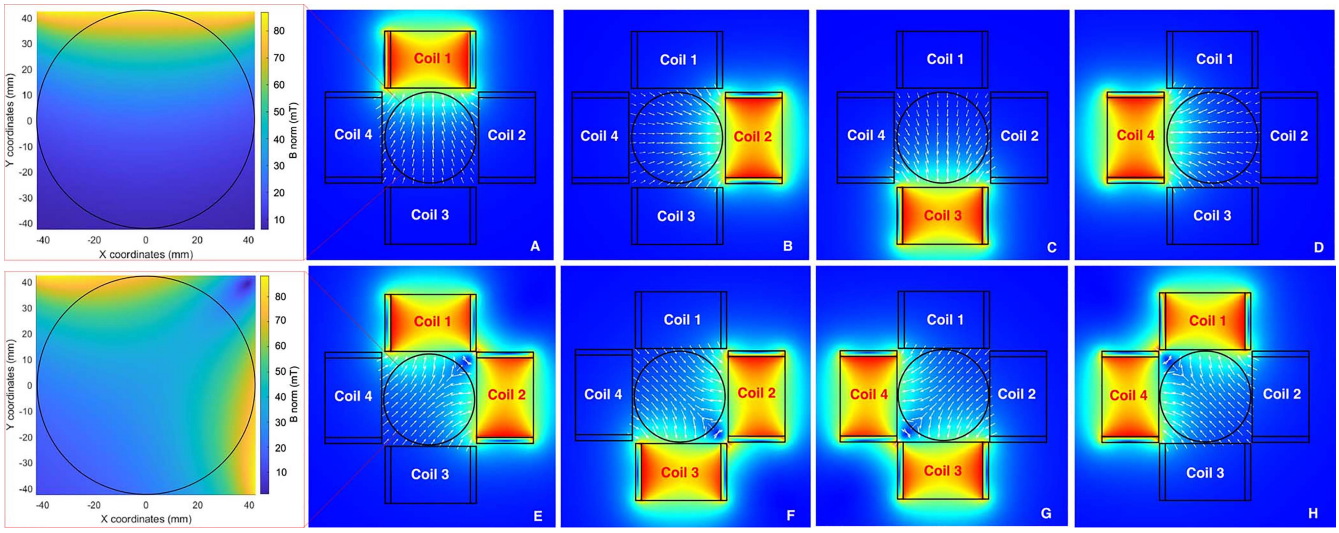

Fig. 8. Magnetic field manipulation for controlling the needle orientation and position in the Petri dish. (A)-(D) Single coil activation for actuating the needle to move in cardinal directions; (E)-(H) Paired coils activation for actuating the needle to move in diagonal directions. The white arrows in the Petri dish area illustrate magnetic field that is represented in logarithmic scale for clear visualization. The magnetic field maps of (A) and (E) in the Petri dish area are presented in the left column.

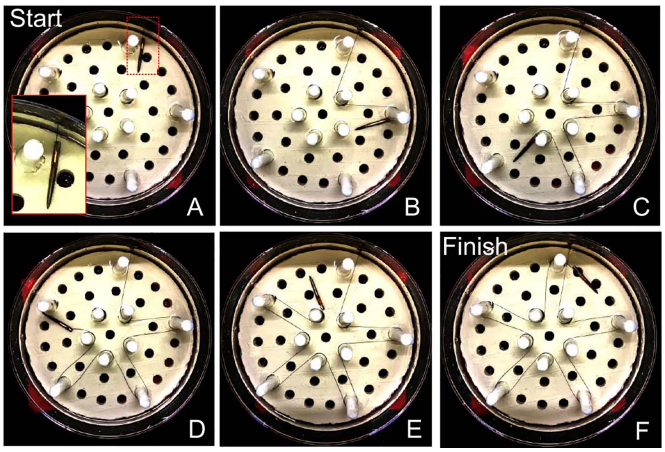

Fig. 9. Purse string pattern was performed using a pentagonal pole geometry and fixed pole positions. (A) Initial position of MagnetoSuture needle, with inset showing the orientation of the sharpened tip of the needle. (B) Coils are energized to move the needle to the interior of the purse string suture, then back to the outer ring, looping around two plastic pegs in the process. (C–E) The purse string pattern is continued, with the needle moving back and forth from interior ring to exterior ring of purse string suture pattern pegs. (F) The needle recovers its original position, having completed loops around all ten pegs.

pulled over ten friction-inducing points of contact using a magnetically guided needle. While the demonstrated purse string suture pattern does not wholly recreate a purse string suture because it lacks repeated tissue penetrations, our goal is to demonstrate precise motion control of a needle and suture thread which can overcome numerous point-of-friction contacts, as well as assess user experience in learning and completing manipulation tasks with the system.

2) Experiment Setup: As shown in Fig. 9, a radially symmetric Petri dish with pentagonally ordered holes was printed and used to hold vertical pegs forming a five-pointed star pattern. The suture thread is threaded through a hole on the sidewall of the Petri dish and rests on a flat surface outside of the coil array. The thread is allowed to be pulled through the sidewall hole with minimum friction outside of the sample region of interest. The tension on the suture thread shown in Fig. 9 is due to the gravitational and small frictional force acting on the suture thread. This purse string suture pattern was used as a test bed for MagnetoSuture steerability as well as force application in the presence of contact friction between suture thread and the vertical pegs.

For understanding and anticipating the movement of magnetic objects in fluids, it is helpful to assess and characterize the forces involved. Our NdFeB needles experience forces due to magnetic field gradients, fluid drag, gravity (ignored due to 2D manipulation), and friction due to needle interactions with Petri dish surface and thread interaction with vertical pegs. Additionally, needles experience torque generated by magnetic fields. Micro/milli-meter scale objects moving in fluidic environments are characterized by dynamics with Reynolds numbers *Re*, which is represented by the ratio of inertial forces to viscous forces as

$$Re = \frac{\rho u D}{\mu}, \tag{2}$$

where D is the dimension of the object, ρ is the fluid density, u represents the object's velocity, and μ denotes the dynamic viscosity of the fluid. Considering a needle with a diameter of 1.6 mm, the needle speed to achieve $Re = 1$ is approximately $5.56 \times 10^2\,\mathrm{mm\,s^{-1}}$ in water (at 25 °C) and approximately $2.49 \times 10^5\,\mathrm{mm\,s^{-1}}$ in polysorbate 80 (at 25 °C) by using (2). The purse string suture experiments were performed in polysorbate 80. This suggests the needle dynamics is with low Reynolds number in the fluidic environments.

In the needle steering experiments, pulling forces and steering torques are applied continuously and cooperatively to position the needle and pull the suture thread through the purse string suture pattern. The magnetic force applied on the needle is formulated in Equation (1), while the magnetic torque applied to the needle is described by

$$\tau = v\mathbf{M} \times \mathbf{B}. \tag{3}$$

TABLE I
SPENT TIME OF EXPERIENCED USES (E) AND NOVICE USERS (N) TO COMPLETE THE PURSE STRING SUTURE PATTERN

Users	Trial 1 (s)	Trial 2 (s)	Trial 3 (s)	Trial 4 (s)	Trial 5 (s)
E1	228	176	144	170	120
E2	232	164	128	134	108
N1	158	108	110	118	134
N2	359	141	198	147	216
N3	243	174	126	96	118

TABLE II
RESULTS OF TWO SAMPLE T-TESTS AT SIGNIFICANCE LEVEL $\alpha = 0.05$

Groups	G1	G2	G3	G4	G5	G6	G7
p	0.07	0.33	0.62	0.28	0.23	0.96	0.91
h	0	0	0	0	0	0	0

For NdFeB magnets (Grade N42), $|\mathbf{M}|$ is approximately $1.08 \times 10^6\,\mathrm{A\,m^{-1}}$. Fig. 9A-F demonstrate the proof of concept completion of a purse string suture pattern incorporating ten "stitch points".

3) User Experience: In order to assess system usability, we tested two experienced users, assessing time required for completion of the purse string suture pattern and comparing completion times with those of three novice users. Experienced users were defined as users who were involved in system design, calibration, and implementation, each of whom had spent more than five hours operating the system. Novice users were selected at random and given 45 minute training sessions. Novice users were trained on patterns other than the purse string suture pattern. The training included moving a NdFeB needle in a circle and a figure eight around two fixed pegs. Each user completed the purse string pattern in five successive trials. The completion times for both experienced and novice users are shown in Table I.

To identify whether significant difference exists between the two groups of users, we conducted two sample t-tests by reasonably assuming 1) the data from experienced and novice users are treated as independent groups; and 2) the data from each group follow a normal distribution without knowing the variance. The seven comparison pairs are generated as G1:(E1, N1), G2:(E1, N2), G3:(E1, N3), G4:(E2, N1), G5:(E2, N2), G6:(E2, N3), and G7:([E1, E2], [N1, N2, N3]). For the last pair G7, we combined all the data from experienced users as one group, and combine all the novice user data as another group. We define the null hypothesis as $H_0 : \mu_E = \mu_N$, which indicates the mean values of the two groups are equal. We run the hypothesis tests based on the significance level of $\alpha = 0.05$. As shown in Table II, the p-values are the levels of marginal significance. The h values suggest accepting (number: 0) or rejecting (number: 1) the null hypothesis. The results indicate that all the tests at $\alpha = 0.05$ accept the null hypothesis. There is no significant difference between the mean values of completion times from experienced and novice users. The results of the statistical analysis suggest that similar performance for NdFeB needle manipulation to those of expert users can be achieved by novice users with short training periods.

B. Tissue Ligation Experiment

The process of ligation requires wrapping a tubular tissue with suture thread with the goal of restricting fluid flow.

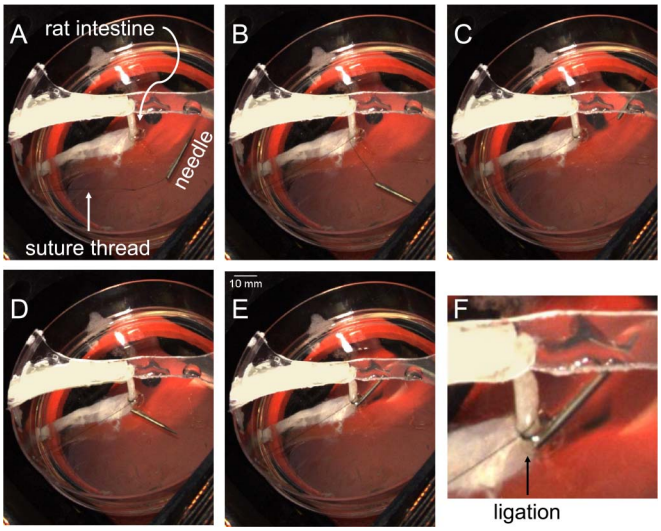

Fig. 10. Tissue ligation procedure. (A) Experiment setup of tissue ligation by fixing a tubular tissue sample vertically. (B) The first encirclement. (C) The second encirclement. (D) The third encirclement. (E) The fourth encirclement. (F) Zoomed in view of tissue ligation.

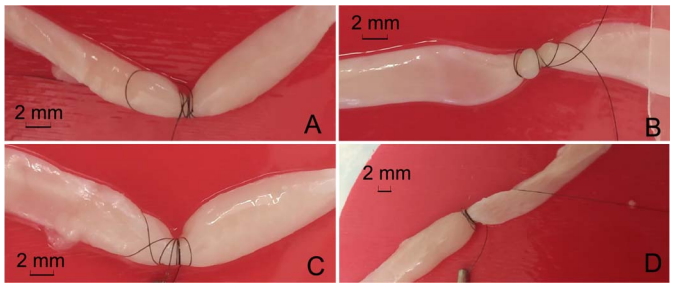

Fig. 11. Repeat ligation experiments in which intestine segments were encircled four times resulted in reduction in tissue diameters by (A) 59.6%, (B) 62.9%, (C) 54.2%, and (D) 53.8%.

Ligation may be performed during surgeries involving arteries of the gastrointestinal tract, for example as a method of restricting blood supply to specific regions of a colon or rectal cancer-containing tissue [41].

To demonstrate ligation, the tissue was mounted in a custom holder which allowed the suture needle to be manipulated around the sample unhindered. The custom holder consisted of concentric Petri dishes, the interior dish having a hole in the center through which rat intestine (BioIVT, Hicksville, New York; www.bioivt.com) was inserted. The rat intestine was attached to an upper support such that the intestine protruded vertically up from the Petri dish. For tissue ligation experiments, the Petri dish was filled with aqueous buffer. To begin ligation, the loose end of the suture thread was tied to the edge of the Petri dish. The needle was then steered in repeated loops around the tissue, drawing the thread tight after each loop was completed, as shown in Fig. 10.

Ligation experiments were performed 4 times, with an average ligation time of 2.4 s/encirclement, with all experiments accomplishing 4 tissue encirclements. The ligation resulted in 59.6% (Fig. 11A), 62.9% (Fig. 11B), 54.2% (Fig. 11C), 53.8% (Fig. 11D) reduction in the tissue diameters respectively.

Fig. 12. NdFeB needle with thread is guided towards suspended rat intestine (A) and pulled through rat intestine (B). Further manipulation pulls suture thread through intestine (C, D), with (E) showing closeup of thread through intestine.

C. Tissue Penetration Experiment

In Section II-B, we have experimentally assessed the required tissue penetration force by a force sensor for designing the electromagnet array in order to generate sufficient penetration force on the NdFeB needle. In this section, we demonstrate tissue penetration using our system.

Intestinal anastomosis is a procedure for reconnecting two distal segments of the intestine, and is often required after removal of an intestinal segment. The procedure typically involves either handsewing or stapling the two segments together, with recent reviews suggesting that handsewing may result in fewer strictures and leaks than stapling the segments together [42]. Here we demonstrate that magnetic gradients can be used to advance a NdFeB needle through a rat intestine tissue using simple cylindrical needles with sharpened tips without the application of rotating, drilling forces.

Fig. 12 shows a segment of *ex vivo* rat intestine used for the tissue penetration experiment. The rat intestine (adult Sprague Dawley rat, BioIVT) was prepared with single-layer and double-layer tissues by spanning the tissues over a custom tissue holder. In order to preserve the mechanical properties of the tissue, the holder is designed to keep the tissue hydrated during experiments by fully submerging the tissue in an aqueous buffer. The suture needle, as illustrated in Fig. 12A and Fig. 12B, was then guided towards and through the sample tissue shown in Fig. 12C–E.

Tissue penetration was attempted four times for single-layer tissues and fourteen times double-layer tissues along the x-axis. For single-layer tissues, the penetration success rate was 100%. Penetration took less than 1 s on average to complete by only using the x-axis electromagnets. For double-layer tissues, the penetration success rate was 57.1%, and took 7.67 s on average for accomplishing penetration by using both x-axis and y-axis electromagnets to induce oscillations in the penetration angle. After each experiment, penetration was confirmed by examination of the tissue, paying specific attention to the location at which the thread went through the tissue.

IV. Discussion

The possibility of removing mechanical manipulators from surgeries offers the potential for truly minimally invasive surgery. The procedures of suturing and ligation inside the body are potentially good candidates for tetherlessly operated surgical tools, as they can be performed with a needle and thread only. Like other forms of robotic surgery, the MagnetoSuture process transfers the strain typically applied by the surgeon's arms, hands, fingers, and tendons from the surgeon and onto control hardware for the application of force. Here, force is applied via electromagnet activation. The presented MagnetoSuture implementation demonstrates preliminary proof of principle success in performing the basic functions of tissue penetration and ligation tasks. Crucially, the MagnetoSuture system concept does not require further insertion of devices aside from the suture needle and thread, significantly reducing the number of devices and amount of device-tissue contact induced during a procedure.

Previous experiments demonstrating magnetically enabled tissue penetration have been accomplished with millimeter scale helical magnetic objects. Rotating magnetic fields with negligible magnetic gradients were used to rotate helices which drilled through tissue. In this work we present a tissue penetration solution by using magnetic field gradient pulling. The presented paradigm of pulling a needle through tissue well-replicates the forces used in natural suturing, which is accomplished primarily with pushing forces applied to smooth, sharpened needles. As the goal of suturing is to bring tissue together to close a wound with minimal damage to sutured tissue, future experiments exploring the damage to tissue based on either gradient pulling or rotating magnetic fields inducing drilling through tissues is warranted.

It is important to distinguish the present work from the broad and growing field of magnetic catheter guidance in terms of the source of the propulsion force. In most catheter guidance work, a distally located magnetic tip or head is steered through tissues, organs, or vasculature using magnetic fields, with propulsion being provided by a tethered drive system which provides insertion forces via a mechanically tethered proximal end [43]. Commercialized medical devices for steering catheters under image guidance currently perform catheter guidance in the operating room with magnetically guided steering and tactile propulsion forces provided by drive motors [44], [45]. New steering systems and flexible magnetic needles for implanting deep brain stimulation electrodes are being developed [34], [46].

Magnetic fields for manipulation have also made their way into the operating room by means of a system for repositioning internal organs/liver during surgery (Levita Magnetics) [47], as well as techniques for recovering needles lost during surgery with magnetic field gradients [48]. One such study used a surgeon-operated articulating laproscopic magnet to reduce the time needed to recover a lost needle by more than 60% [49]. These recent developments point to the growing potential for using well-designed magnetic fields and magnetic surgical tools to simplify, advance, or increase the safety of operating room procedures.

While our demonstrations represent an advance in the field of magnetically guided suture procedures, numerous limitations to the system exist. The choice of orthogonally arranged electromagnets in a 2D configuration offers advantages and drawbacks. For simple 2D flat arrangements of electromagnets, Erni *et al.* previously demonstrated that arrays of eight identically sized coils offered more uniform field strength across a region of interest, however due to the extra space needed to position all eight coils, resulted in lower overall field within the region of interest [50]. As procedures such as ligation and tissue penetration require maximum force and gradient, we opted for a four-coil array. While the sample region region was easy to access and visualize, manipulations were essentially limited to a plane. As such, other coil array geometries will be required for expanding the control, force, and region of operation capabilities of the system. Additional challenges arise in attempts to scale the MagnetoSuture construct to human-scale dimensions. Pulsed power and use of specialized core materials may mitigate such challenges. Future experiments may implement arrangements including sufficient number of coils to generate a broader range of motions in 3D. Additionally, arrays of capacitors or batteries could be implemented so as to supply hundreds of amperes of current to the coils for short periods [51], significantly improving the range of forces accessible to the system.

Challenges in visualization and image guidance also exist. Our system uses an optical image based feedback scheme which allows a human-in-the-loop controller to steer the suture needle via a wireless remote controller. However, for interventions in the GI tract, minimally invasive practice makes use of an endoscope for imaging. Thus, methods for operating in confined spaces with on-board imaging will be required for eventual application of such a paradigm.

Further improvements in the area of control and automation are also possible. Specifically, automated needle tracking and real time force feedback may be implemented for providing the operator with a tactile sense of the tissue environment. Future implementations may not be tied to the use of joystick-based control methods, and would significantly benefit from force-feedback manipulation.

Needle size and sharpness are critical parameters for successfully penetrating tissue, and the shape of the needle tip and diameter of the needle determine the amount of force required to successfully move the needle through tissue. After sharpening, NdFeB needles had a radius of curvature $>$3x the radius of curvature of Ethicon ST-4 needles (98 μm for NdFeB needles as compared with 30 μm for commercial ST-4 needles, see Figure 2). We anticipate improvements in techniques for sharpening NdFeB needles may lead to a $>$50% reduction in the required force for penetration. Additionally, needles used in our experiments were N42 grade NdFeB magnets with residual induction, $B_{r(max)}$, of 1.32 T. Using N52 grade NdFeB needles would offer $B_{r(max)}$ of 1.48 T, a 12% increase in the residual induction and a corresponding increase in force due to an applied magnetic field gradient. Increases in the supplied magnetic fields and field gradients, along with sharper needles made of N52 grade NdFeB, will significantly expand the types and thicknesses of tissues which can be penetrated. A major drawback for magnetic gradient induced needle manipulation is that the applied magnetic force and damage to the involved tissues both scale with volume. Thus, a larger needle becomes easier to manipulate and supports application of larger forces, but also causes more tissue damage and meets significant resistance to tissue penetration due to its size. Balancing the need for large forces while minimizing tissue damage, as well as having a needle diameter that can readily penetrate tissues poses a unique challenge for gradient driven magnetic operations. Our choice in needle dimensions was driven by the need for the smallest diameter NdFeB cylinder we could effectively sharpen using readily available tools and also apply sufficient force to accomplish the described tasks. Efforts to further sharpen a thinner, N52 grade cylindrical magnet will likely result in decreased rupture forces and increases in surgical usefulness. It is possible that needle length could be substituted for needle diameter to allow for sufficient magnetic material for transferring the force necessary for a given operation. Long, thin needles may be useful for operations in which tissue damage should be avoided but ample linear space is available for manipulation of longer needles.

While using magnetic field gradients to guide suture needles is an inherently unstable approach, we are aware of no physical limits to using it as a method of manipulation for generating highly controlled motions. We see opportunities for advancing the field by better understanding such instabilities. The instabilities induced in needle translation must be accounted for and understood, and advanced control methods must be developed. We acknowledge that the applicability of such a technique to human-scale interventions is heavily dependent upon advances in control, pulse shaping, field generation, force feedback, and imaging of such manipulations. Additionally, a more complete understanding of local tissue dynamics, in real time and with high imaging frequency and resolution, will be required to move such demonstrations from the bench to the bedside.

V. Conclusion

A simple four coil system capable of manipulating a permanent magnet suture needle has been presented, and analogs of surgical procedures have been demonstrated. The design is capable of supplying sufficient force and torque to move a needle with attached suture thread through a suture pattern by human-in-the-loop control. Ligation of *ex vivo* tissue was demonstrated using rat intestine, and tissue penetration was demonstrated. Future work will expand system capabilities by adding out-of-plane coils for three-dimensional manipulation, increasing coil separation so as to fit an anesthetized rat, and increasing current capabilities for generating stronger field and gradients. Additionally, future work will implement vision-based feedback control for autonomous control of the suture needle.

References

[1] C. Tsui, R. Klein, and M. Garabrant, "Minimally invasive surgery: National trends in adoption and future directions for hospital strategy," *Surg. Endoscopy*, vol. 27, no. 7, pp. 2253–2257, 2013.

[2] T. G. Weiser *et al.*, "An estimation of the global volume of surgery: A modeling strategy based on available data," *Lancet*, vol. 372, no. 9633, pp. 139–144, 2008.

[3] D. Mackenzie, "The history of sutures," *Med. History*, vol. 17, no. 2, pp. 158–168, 1973.

[4] S. A. Antoniou, R. Pointner, and F. A. Granderath, "Single-incision laparoscopic cholecystectomy: A systematic review," *Surg. Endoscopy*, vol. 25, no. 2, pp. 367–377, 2011.

[5] R. S. Chamberlain and S. V. Sakpal, "A comprehensive review of single-incision laparoscopic surgery (SILS) and natural orifice translu-minal endoscopic surgery (NOTES) techniques for cholecystectomy," *J. Gastrointestinal Surg.*, vol. 13, no. 9, pp. 1733–1740, 2009.

[6] S. Maeso *et al.*, "Efficacy of the Da Vinci surgical system in abdominal surgery compared with that of laparoscopy," *Ann. Surg.*, vol. 252, no. 2, pp. 254–262, 2010.

[7] A. Shademan, R. S. Decker, J. D. Opfermann, S. Leonard, A. Krieger, and P. C. W. Kim, "Supervised autonomous robotic soft tissue surgery," *Sci. Transl. Med.*, vol. 8, no. 337, 2016, Art. no. 337ra64. [Online]. Available: http://stm.sciencemag.org/cgi/doi/10.1126/scitranslmed.aad9398

[8] G. Gandaglia *et al.*, "Effect of minimally invasive surgery on the risk for surgical site infections: Results from the national surgical quality improvement program (NSQIP) database," *JAMA Surg.*, vol. 149, no. 10, pp. 1039–1044, Oct. 2014.

[9] A. K. Salem, P. C. Searson, and K. W. Leong, "Multifunctional nanorods for gene delivery" *Nat. Mater.*, vol. 2, no. 10, pp. 668–671, Oct. 2003. [Online]. Available: http://www.ncbi.nlm.nih.gov/pubmed/12970757

[10] L. O. Mair and R. Superfine, "Single particle tracking reveals biphasic transport during nanorod magnetophoresis through extracellular matrix," *Soft Matter*, vol. 10, no. 23, pp. 4118–4125, Apr. 2014. [Online]. Available: http://www.ncbi.nlm.nih.gov/pubmed/24744160

[11] A. Ghosh and P. Fischer, "Controlled propulsion of artificial magnetic nanostructured propellers," *Nano Lett.*, vol. 9, no. 6, pp. 2243–2245, Jun. 2009. [Online]. Available: http://www.ncbi.nlm.nih.gov/pubmed/19413293

[12] L. Zhang, K. E. Peyer, and B. J. Nelson, "Artificial bacterial flagella for micromanipulation," *Lab Chip*, vol. 10, no. 17, pp. 2203–2215, Sep. 2010. [Online]. Available: http://www.ncbi.nlm.nih.gov/pubmed/20567752

[13] K. E. Peyer, S. Tottori, F. Qiu, L. Zhang, and B. J. Nelson, "Magnetic helical micromachines," *Chem. Eur. J.*, vol. 19, no. 1, pp. 28–38, 2013.

[14] K. E. Peyer, L. Zhang, and B. J. Nelson, "Localized non-contact manipulation using artificial bacterial flagella," *Appl. Phys. Lett.*, vol. 99, no. 17, 2011, Art. no. 174101. [Online]. Available: http://link.aip.org/link/APPLAB/v99/i17/p174101/s1&Agg=doi

[15] L. Zhang *et al.*, "Controlled propulsion and cargo transport of rotating nickel nanowires near a patterned solid surface," *ACS Nano*, vol. 4, no. 10, pp. 6228–6234, Oct. 2010. [Online]. Available: http://www.ncbi.nlm.nih.gov/pubmed/20873764

[16] L. Zhang, T. Petit, K. E. Peyer, and B. J. Nelson, "Targeted cargo delivery using a rotating nickel nanowire," *Nanomed. Nanotechnol. Biol. Med.*, vol. 8, no. 7, pp. 1074–1080, Mar. 2012. [Online]. Available: http://www.ncbi.nlm.nih.gov/pubmed/22426194

[17] L. Mair *et al.*, "Magnetically aligned nanorods in alginate capsules (MANiACs): Soft matter tumbling robots for manipulation and drug delivery," *Micromachines*, vol. 10, no. 4, p. 230, 2019.

[18] M. Sitti *et al.*, "Biomedical applications of untethered mobile milli/microrobots," *Proc. IEEE*, vol. 103, no. 2, pp. 205–224, Feb. 2015.

[19] J. Li, B. E.-F. de Ávila, W. Gao, L. Zhang, and J. Wang, "Micro/nanorobots for biomedicine: Delivery, surgery, sensing, and detoxification," *Sci. Robot*, vol. 2, no. 1, pp. 1–10, 2017.

[20] C. Chautems, B. Zeydan, S. Charreyron, G. Chatzipirpiridis, S. Pané, and B. J. Nelson, "Magnetically powered microrobots: A medical revolution underway?" *Eur. J. Cardio thoracic Surg.*, vol. 51, no. 3, pp. 405–407, 2017.

[21] O. Ergeneman, C. Bergeles, M. P. Kummer, J. J. Abbott, and B. J. Nelson, "Wireless intraocular microrobots: Opportunities and challenges," in *Surgical Robotics: Systems Applications and Visions*, 1st ed., J. Rosen, B. Hannaford, and R. M. Satava, Eds. Boston, MA, USA: Springer, 2011, pp. 271–311.

[22] S. Fusco *et al.*, "Microrobots: A new era in ocular drug delivery," *Expert Opin. Drug Del.*, vol. 11, no. 11, pp. 1815–1826, 2014.

[23] C. Pappone *et al.*, "Robotic magnetic navigation for atrial fibrillation ablation," *J. Amer. College Cardiol.*, vol. 47, no. 7, pp. 1390–1400, 2006.

[24] B. L. Nguyen, J. L. Merino, and E. S. Gang, "Electrophysiology navigation: Remote navigation for ablation procedures—A new step forward in the treatment of cardiac arrhythmias," *Eur. Cardiol.*, vol. 6, no. 3, pp. 50–56, 2010.

[25] C. Chautems and B. J. Nelson, "The tethered magnet: Force and 5-DoF pose control for cardiac ablation," in *Proc. IEEE Int. Conf. Robot. Autom. (ICRA)*, 2017, pp. 4837–4842.

[26] T. Honda, K. I. Arai, and K. Ishiyama, "Micro swimming mechanisms propelled by external magnetic fields," *IEEE Trans. Mag.*, vol. 32, no. 5, pp. 5085–5087, Sep. 1996.

[27] K. Ishiyama, M. Sendoh, A. Yamazaki, and K. I. Arai, "Swimming micro-machine driven by magnetic torque," *Sensors Actuators A, Phys.*, vol. 91, nos. 1–2, pp. 141–144, 2001.

[28] J. Rahmer, C. Stehning, and B. Gleich, "Remote magnetic actuation using a clinical scale system," *PLoS ONE*, vol. 13, no. 3, 2018, Art. no. e0193546.

[29] K. Ishiyama, M. Sendoh, and K. I. Arai, "Magnetic micromachines for medical applications," *J. Magn. Magn. Mater.*, vols. 242–245, pp. 41–46, Apr. 2002.

[30] M. Sendoh, Y. Suda, K. Ishiyama, and K. I. Arai, "Fabrication of magnetic actuator for use in colon endoscope," in *Proc. Int. Symp. Micromechatron. Human Sci. (MHS)*, vol. 39, 2003, pp. 165–170.

[31] A. W. Mahoney, N. D. Nelson, E. M. Parsons, and J. J. Abbott, "Non-ideal behaviors of magnetically driven screws in soft tissue," in *Proc. IEEE Int. Conf. Intell. Robots Syst.*, 2012, pp. 3559–3564.

[32] N. D. Nelson, J. Delacenserie, and J. J. Abbott, "An empirical study of the role of magnetic, geometric, and tissue properties on the turning radius of magnetically driven screws," in *Proc. IEEE Int. Conf. Robot. Autom.*, 2013, pp. 5372–5377.

[33] J. Leclerc, A. Ramakrishnan, N. V. Tsekos, and A. T. Becker, "Magnetic hammer actuation for tissue penetration using a millirobot," *IEEE Robot. Autom. Lett.*, vol. 3, no. 1, pp. 403–410, Jan. 2018.

[34] A. J. Petruska *et al.*, "Magnetic needle guidance for neurosurgery: Initial design and proof of concept," in *Proc. IEEE Int. Conf. Robot. Autom.*, Jun. 2016, pp. 4392–4397.

[35] X. Bao, W. Li, M. Lu, and Z. Zhou, "Experiment study on puncture force between MIS suture needle and soft tissue," *Biosurface Biotribol.*, vol. 2, no. 2, pp. 49–58, 2016.

[36] P. R. Cohen, P. T. Martinelli, K. E. Schulze, and B. R. Nelson, "The purse-string suture revisited: A useful technique for the closure of cutaneous surgical wounds," *Int. J. Dermatol.*, vol. 46, no. 4, pp. 341–347, 2007.

[37] N. K. Weisberg and S. S. Greenbaum, "Revisiting the purse-string closure: Some new methods and modifications," *Dermatologic Surg.*, vol. 29, no. 6, pp. 672–676, 2003.

[38] A. J. Drakeley, D. Roberts, and Z. Alfirevic, "Cervical cerclage for prevention of preterm delivery: Meta-analysis of randomized trials," *Obstetrics Gynecol.*, vol. 102, no. 3, pp. 621–627, 2003.

[39] A. H. Ostergaard, "A simple technique for closure of temporary cystostomy," *Surg. Gynecol. Obstetrics*, vol. 142, no. 6, pp. 915–916, 1976.

[40] C. Tremolada, D. Blandini, M. Beretta, and M. Mascetti, "The 'round block' purse-string suture: A simple method to close skin defects with minimal scarring," *Plastic Reconstructive Surg.*, vol. 100, no. 1, pp. 126–131, 1997.

[41] M. Zerey, L. M. Hawver, Z. Awad, D. Stefanidis, W. Richardson, and R. D. Fanelli, "SAGES evidence-based guidelines for the laparoscopic resection of curable colon and rectal cancer," *Surg. Endoscopy*, vol. 27, no. 1, pp. 1–10, 2013.

[42] A. Nordholm-Carstensen, M. S. Rasmussen, and P. M. Krarup, "Increased leak rates following stapled versus handsewn ileocolic anastomosis in patients with right-sided colon cancer: A nationwide cohort study," *Diseases Colon Rectum*, vol. 62, no. 5, pp. 542–548, 2019.

[43] B. S. Yeow and R. Hongliang, "Magnetic actuated catheterization robotics," in *Electromagnetic Actuation and Sensing in Medical Robotics*, H. Ren and J. Sun, Eds. Singapore: Springer, 2018, pp. 73–103.

[44] S. Ramcharitar, M. S. Patterson, R. J. van Geuns, C. van Meighem, and P. W. Serruys, "Technology Insight: Magnetic navigation in coronary interventions," *Nat. Clin. Pract. Cardiovascular Med.*, vol. 5, no. 3, pp. 148–156, 2008.

[45] L. Muller, M. Saeed, M. W. Wilson, and S. W. Hetts, "Remote control catheter navigation: Options for guidance under MRI," *J. Cardiovascular Magn. Reson.*, vol. 14, no. 1, pp. 1–9, 2012.

[46] A. Hong, Q. Boehler, R. Moser, A. Zemmar, L. Stieglitz, and B. J. Nelson, "3D path planning for flexible needle steering in neurosurgery," *Int. J. Med. Robot. Comput. Assist. Surg.*, vol. 15, no. 4, 2019, Art. no. e1998.

[47] H. Rivas *et al.*, "Magnetic surgery: Results from first prospective clinical trial in 50 patients," *Ann. Surg.*, vol. 267, no. 1, pp. 88–93, 2018.

[48] R. Jayadevan, K. Stensland, A. Small, S. Hall, and M. Palese, "A protocol to recover needles lost during minimally invasive surgery," *J. Soc. Laparoendoscopic Surgeons*, vol. 18, no. 4, 2014, Art. no. e2014.

[49] A. C. Small, D. M. Gainsburg, M. A. Mercado, R. E. Link, S. P. Hedican, and M. A. Palese, "Laparoscopic needle-retrieval device for improving quality of care in minimally invasive surgery," *J. Amer. College Surgeons*, vol. 217, no. 3, pp. 400–405, 2013, doi: 10.1016/j.jamcollsurg.2013.02.035.

[50] S. Erni, S. Schürle, A. Fakhraee, B. E. Kratochvil, and B. J. Nelson, "Comparison, optimization, and limitations of magnetic manipulation systems," *J. Micro Bio Robot.*, vol. 8, nos. 3–4, pp. 107–120, 2013.

[51] C. Ropp *et al.*, "Electropermanent magnets for variable-field NMR," *J. Magn. Reson.*, vol. 303, pp. 82–90, Jun. 2019. [Online]. Available: https://doi.org/10.1016/j.jmr.2019.04.010